Current state-of-the-art of hydrogen trapping by carbides: from theory to experiment

Liese Vandewalle[1], Tom Depover[1]*, Kim Verbeken[1]*

[1] Ghent University, Department of Materials, Textiles and Chemical Engineering, Sustainable Materials Science, Tech lane Ghent Science Park 46, B-9052 Ghent, Belgium
Liese.Vandewalle@UGent.be
Tom.Depover@UGent.be (+3293310438)
Kim.Verbeken@UGent.be (+3293310453)
*corresponding authors

Abstract

This study reviews the interactions of hydrogen with carbides. Often, the introduction of well-chosen carbides is suggested as a strategy in the development of steels with higher resistance against hydrogen embrittlement. However, despite numerous experimental studies published in literature, many uncertainties and discrepancies still exist regarding their potential beneficial effect. This could be related to differences in carbide/matrix interface character, chemical composition, carbide distribution or even charging and/or mechanical loading conditions, which all affect the hydrogen trapping characteristics and thus the hydrogen distribution in the steel specimens. Consequently, advanced insights in the fundamental aspects of the hydrogen trapping by the different sites provided by carbides are of high importance. In this paper, the fundamental insights obtained by theoretical calculations is reviewed and linked to experimental observations reported in literature, as such alleviating some of the reported discrepancies and revealing new insights in the hydrogen-carbide interactions.

keywords: Hydrogen trapping; carbides; steel; first principle calculations; hydrogen mapping techniques; thermal desorption spectroscopy;

1 Introduction

The use of hydrogen gas as an energy carrier is considered one of the most important strategies to reduce the CO_2 emissions and achieve a sustainable future. Unfortunately, the use of hydrogen also comes with considerable issues, such as hydrogen embrittlement (HE) of steels, strongly complicating the safe transport and storage of the H_2 gas. A possible strategy to enhance a steel's resistance against HE considers the introduction of well-designed hydrogen (H) traps in the steel microstructure. In this perspective, carbides are reported to be of large interest, as they are readily added to steels for their significant strengthening effect, and as discussed later, may provide many different H trapping sites. Indeed, the strong resistance against HE of high-strength low-alloy (HSLA) steels compared to different industrial high-strength steels was related to the presence of titanium (Ti) and Niobium (Nb) based precipitates [1, 2]. Numerous studies have been performed on the influence of the carbide presence in a steel microstructure on the HE for various types of carbides.

Lee et al. [3] evaluated the influence of chromium (Cr), molybdenum (Mo) and vanadium (V) carbides on the HE resistance of pre-charged tempered martensitic steels. They found that precipitation of Cr-rich M_7C carbides did not provide a beneficial effect on the HE of the steel. On the other hand, fine plate-like VC and nano-sized Mo carbides were found to considerably improve the HE resistance. While the V carbide-containing steel showed the best performance in the slow strain rate tests, the large H

uptake by these carbides raised questions about their use in practical applications. The Mo-carbides were indicated as the most promising because of their low H uptake from corrosive environment in combination with a high critical H content. Fracture toughness and fatigue crack growth tests performed by Peral et al. [4] on specimens pre-charged with H indicated that the presence of fine (V,Mo) carbides clearly decreased the HE susceptibility. In the fatigue tests, the presence of these carbides even resulted in a negligible effect upon H pre-charging, even though they increased the initial H uptake. Larger Fe-Cr-Mo mixed carbides, on the other hand, still resulted in significant HE. Depover et al. [5] compared the effect of Cr, Mo and Ti precipitation on the HE of steels with a tempered martensitic microstructure. They noted that the TiC performed worst, even increasing the HE susceptibility, while Mo-containing steel showed the highest resistance. Contrary, Kim et al. [6] observed an improvement in HE resistance with addition of Ti to hot stamped boron steels, which they related to the beneficial effect of TiC to HE. Nagao et al. [7] also observed an improvement of the HE in bending samples upon the addition of Ti, due to the precipitation of (Ti,Mo)C. This discrepancy was elucidated by Depover and Verbeken in a later study [8], showing that the increase in percentage HE upon TiC precipitation could be linked to a much higher H amount introduced during the charging procedure. When altering the charging procedure in order to keep the amount of H constant, the presence of precipitated TiC clearly reduced the HE, revealing their beneficial effect.

Additionally, multiple studies considered the role of carbide size and distribution. A homogeneous distribution of carbides was reported by dos Santos et al. [9] to result in lower HE susceptibility compared to a heterogeneous carbide distribution. Lee et al. [10] found that the presence of fine vanadium carbides resulted in an enhancement of the HE resistance while large undissolved V-based carbides led to brittle fracture and increased the HE susceptibility. Seo et al. [11] studied the evolution of the HE resistance as a function of tempering time of a V-containing steel. They found that the highest resistance corresponded to the peak ageing condition, i.e. the tempering time resulting in the highest precipitation hardening. Depover and Verbeken [12] also indicated an increased HE susceptibility with increasing amount and size of the vanadium carbides in tempered martensitic steels. Similarly, for TiC the beneficial effect of the carbides was indicated to decrease with increasing size [8]. Conversely, for Cr-containing steels, prolonging the tempering time resulted in lower values of HE index.

These differences were often related to the trapping characteristics of the carbides, typically involving trap density and trap strength. The strength of trapping can be linked to the binding energy (E_B) of hydrogen or the de-trapping activation energy (E_a). Additionally, the occupation of the trapping sites might also be influenced by the energy barrier to enter the carbides (E_t). Depover et al. [13] stated that the HE was most strongly correlated to the mobile H present in the material. This mobile H could easily move towards critical sites in the microstructure such as the dislocations and assist in the cracking process, leading to significant ductility reductions. By providing trapping sites, i.e. sites in the microstructure with lower energy for H compared to the lattice, the carbides can retard H migration through the bulk and act as sinks, storing significant amounts of H, which leads to lower mobile H concentrations. However, Dadfarnia et al. [14] indicated that the introduction of trapping sites is not a valid strategy in the case of open systems, i.e. where there is a continuous supply of H. Over time, the traps get saturated and hence become useless in protection of the critical microstructural sites. On the other hand, Fernández-Sousa et al. [15] argued that this might be the case for static loading, but in the case of dynamic fatigue loading, the presence of traps might be beneficial in both open and closed systems. They stated that the maximum H concentration ahead of the crack tip is sensitive to the ratio of the effective diffusion coefficient over the loading frequency. Thus, increasing the density of trapping sites related to carbides reduces the maximum H concentration attained for a given frequency and extends the regime of safe frequencies. An increase in E_B-value is also stated to reduce

the effective diffusivity and thus improve the safe fatigue behavior. However, it was stated that the effect of the binding energy is smaller than the effect of trap density.

Additionally, the H trapping by carbides might also cause significant H segregation, leading to blister nucleation and crack formation. Some carbides could indeed act as blister initiation sites, such as TiC [16] and large incoherent NbC [17], while others were shown to be less prone to blister initiation [16] or even inhibited blister nucleation by minimizing H segregation at other microstructural features acting as initiation sites [17]. For example, Zhang et al. [17] indicated that few nano-sized NbC considerably retarded blister nucleation due to the inhibition of H segregation at inclusions, which were the active blister nucleation sites.

Clearly, understanding of the interactions of H with carbides and their defects is of major importance. Generally, the trapping sites related to carbides are divided according to the region they occur, i.e. the elastic strain field in the matrix surrounding the carbide, the matrix/carbide interface, and the carbide bulk, as is visualized in Figure 1. The elastic strain field induced in the matrix by the presence of the carbide is generally rather weak and has been shown to provide only limited attraction for the H atoms [18]. The other two, the interface and bulk, may act as preferential sites for H accumulation or may contain defects that interact with H. Therefore, the H interactions in these regions are further discussed in the following sections. First, the results from theoretical calculations on trapping at the carbide/matrix interface and in the carbide bulk is discussed. Next, a review of the experimental characterization of these interactions is presented which reevaluates some of the reported results with the additional insights from first-principle calculations. Finally, the main conclusions are summarized, remaining knowledge gaps are pointed out and suggestions for further studies are made.

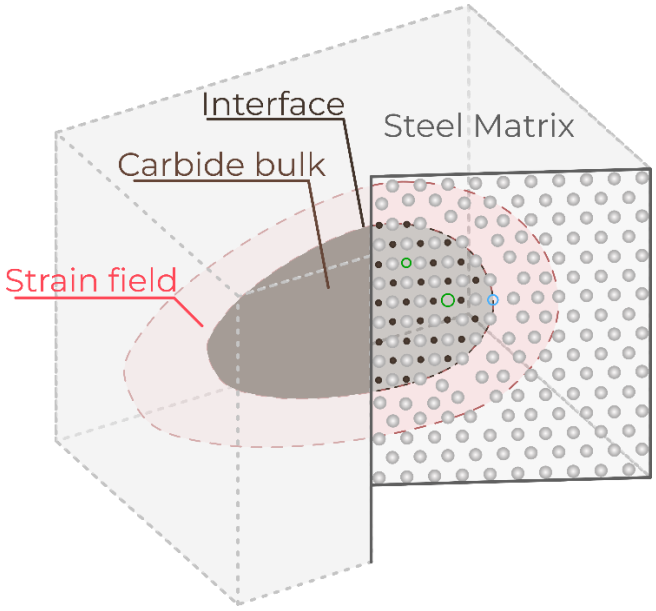

Figure 1: Schematic representation of different trapping sites related to a carbide. Black and grey dots represent non-metal and metal atoms, respectively. Green indicates a defect site in carbide bulk while blue is related to the interface.

2 Insights from theoretical calculations

2.1 Hydrogen interactions at the carbide bulk

Similarly to the iron lattice, H may reside in the interstitial sites of the carbide lattice. Since the iron and carbide lattice differ considerably, they contain significantly different energy sites for H. For some carbides, such as the Cr_7C_3 [19], the interstitial positions in the carbide are energetically more favorable than those in the iron lattice. Hence, H might segregate in the bulk of these carbides. However, considerable accumulation of H in the bulk carbide requires H migration through the bulk. Krause et al. [19] demonstrated that H migration in Cr_7C_3 corresponds to high energy barriers. Consequently, the high migration barrier could inhibit H segregation in the interior of large carbides, despite the presence of the low-energy sites. Similarly, Kawakami and Matsumiya [20] indicated that while the interstitial sites in cementite showed a binding energy of 41 kJ/mol (0.42 eV), the H migration energy through the cementite lattice was found to be 59 kJ/mol (0.61 eV), which was considered too high for considerable H diffusion and hence, uptake in the cementite lattice.

For most carbides, the interstitial positions are considerably higher in energy than the normal iron lattice sites as observed by DFT calculations [19, 21, 22]. Especially perfect transition metal carbides of the MC structure were reported to show very high solution energies [18, 21-25]. This high solution enthalpy of the MC carbides was related by Hickel et al. [21] to the stable structure of the carbides, where the octahedral sites of the metal lattice are already filled with carbon and contain many covalent bonds. As a result, the insertion of H in the carbide lattice destabilizes the bonds, hence increasing the energy. While for M_7C_3-type carbides, Krause et al. [19] implied that the solution enthalpy was related to the atomic volume at the interstitial site, i.e. the sites with largest volume showed the lowest solution enthalpy. However, they also noted the influence of the presence of carbon atoms (C), as the lowest energy sites were typically related to the sites with no C first neighbors.

Despite the high calculated solution energies, experimental observations of H at the bulk of carbides have been reported [26-33]. While these experiments are discussed in section 3, it could be noted that H trapping at the bulk could be related to the presence of defects in the carbide lattice. Two types of defects can be present in the metal carbide particles, i.e. the C-vacancy and the metal-vacancy. Ma et al. [22] studied the effect of these defects on H trapping in VC and NbC using first principle calculations. They showed that the C-vacancy always acted as a stable trapping site while the metal-vacancy only acted as a weak trap. Sagar et al. [34] reported that metal-vacancies in NbC, VC, and TiC were highly unfavorable for H segregation, but confirmed the strong trapping character of the C-vacancies. Various DFT studies concerning the trapping of H at C-vacancy for different carbide types have been reported in literature [18, 22, 24, 25, 34-36]. Figure 2 gives an overview of the results reported in literature. Clearly, the strongest trapping is observed by the C-vacancies in the TiC, along with the C-vacancies in HfC and ZrC, while TaC, NbC, and VC showed rather low binding energies with the C-vacancies.

Moreover, Hammer et al. [24] indicated that the trapping capacity of the C-vacancy in the TiC is strongly influenced by the local chemical environment. Changing the composition from pure TiC to mixed (Ti,V)C strongly decreased the binding energy related to the C-vacancy. Also, (partially) replacing the C atoms by nitrogen (N) atoms resulted in lower binding energies, indicating that a non-metal vacancy in the bulk of titanium nitrides and carbonitrides provided weaker traps than in pure TiC. For vanadium the opposite effect was observed, i.e. the non-metal vacancy in VN was found to provide stronger trapping than in VC [22, 24]. The presence of C-vacancies leads to a sub-stoichiometry of the carbide, i.e. the chemical position can be written as MC_x with $x<1$ or M_yC_x with $y/x>1$. Consequently, the symmetry of the carbide lattice might be strongly affected. Additionally, the influence of the C-

vacancy concentration on the H binding energies has been studied since these carbides are known to show deviations from stoichiometry. Especially, vanadium carbides have been reported to contain a high amount of C-vacancies and are often present in steels as V_4C_3. Huang et al. [37] evaluated the influence of this change in C-vacancy concentration for the H trapping in vanadium carbides. Their results are summarized in Table 1. Clearly, the stoichiometry and structure of the vanadium carbides strongly influence the H trapping capacity. On the other hand, Di Stefano et al. [25] reported no change in binding energy when the C-vacancies in titanium carbides become clustered. Salehin et al. [36] performed a detailed study on the evolution of H binding energy upon C loss for various types of carbides. They reported that indeed for titanium carbides together with hafnium and zirconium carbides the trapping is relatively insensitive to the C-vacancy concentration in the range of 0.5 to 0.325 C atomic fraction. However, H trapping at the C-vacancies in the vanadium, niobium and tantalum carbides showed a strong dependency on the C fraction in the range of 0.5 to 0.4. The binding energy first decreased when going from a mono-vacancy in the carbide to a C fraction of 0.467 and further increased with decreasing C fraction, i.e. increasing vacancy concentration. For a C fraction of 0.4, corresponding to a M_3C_2 structure, strong trapping could even be expected with binding energies up to 0.75 eV for vanadium and niobium carbides.

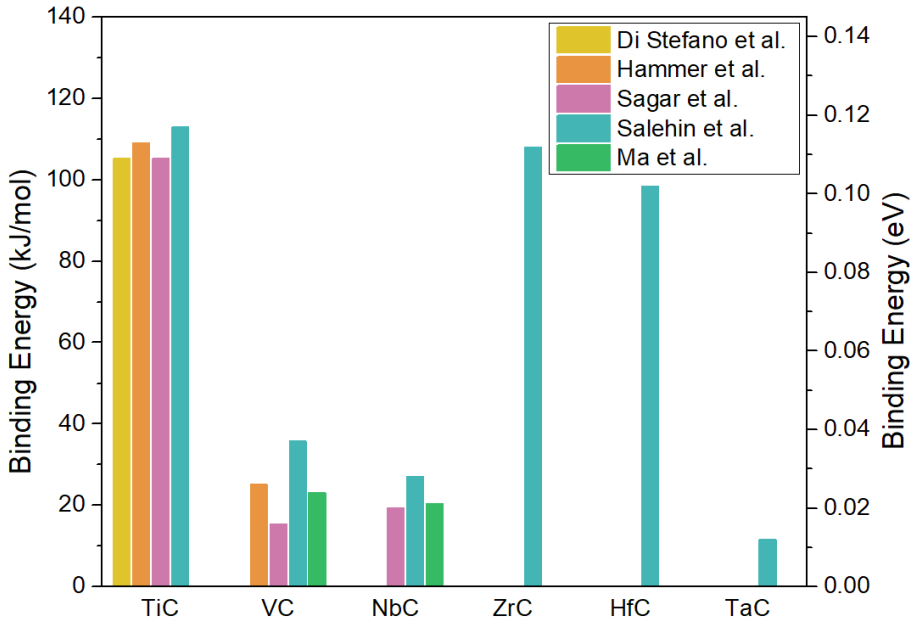

Figure 2: Overview of the H binding energies to the C-vacancy in various different transition metal carbides (MC) according to DFT calculations performed by Di Stefano et al. [25], Sagar et al. [34], Salehin et al. [36], Hammer et al. [24] and Ma et al. [22].

As mentioned earlier, substantial bulk trapping requires H migration through the carbides. Li et al. [23] reported interstitial H migration barriers in transition metal carbides ranging between 19.9 kJ/mol (0.206 eV) and 27.4 kJ/mol (0.284 eV), with TiC exhibiting the highest migration barrier and VC the lowest. While these values might be considered reasonable, one must also consider that H typically originates in the iron lattice and must, therefore, first be able to enter the carbide. Due to the high energy values at the interstitial sites, and possibly low energy sites at the carbide/matrix interface, entry into the carbides usually involves very high energy barriers. Consequently, the C-vacancies can be considered as traps with high E_B but also an extremely high E_t. The presence of C-vacancies can further hinder diffusion through the carbide because of their trapping effect, as indicated by Ding et al. [35] for titanium carbides and by Huang et al. [37] for vanadium carbides. On the other hand, the presence of connected vacancies could lower the diffusion barrier. For example, Di Stefano et al. [25]

reported that H migration in a TiC from one C-vacancy site to a connected C-vacancy site corresponded to an energy barrier of 114.8 kJ/mol (1.19 eV), compared to energy barriers above 180 kJ/mol for isolated C-vacancies. Ding et al. [35] obtained an energy barrier of 118.7 kJ/mol (1.23 eV) for connected C-vacancies and up to 361 kJ/mol (3.74 eV) when the C-vacancy concentration is low. Similarly, Huang et al. [37] reported a decrease in the H migration energy from 205 kJ/mol (2.12 eV) to 93 kJ/mol (0.96 eV) when changing the structure from V_4C_3 to V_2C. Consequently, questions may arise regarding the possibility of H absorption in the bulk of large carbides at room temperature.

Table 1: Binding energies of hydrogen to carbon vacancies in different types of vanadium carbides (V_yC_x), based on values of Huang et al. [37] considering a heat of solution of 20.3 kJ/mol as reported by Ma et al. [22]. Values in brackets were obtained by Kawakami and Matsumiya [18].

V_yC_x	Symmetry Group	E_B (kJ/mol)	E_B (eV)
V_8C_7	$P4_332$	23.1	0.239
V_6C_5	$P3_1$	34.7	0.360
V_4C_3	R-3m	133.6 (116)	1.385 (1.202)
V_2C	Pbcn	70.1	0.727

2.2 Hydrogen interactions at the carbide/matrix interface

Hydrogen trapping at the carbide/matrix interface is strongly influenced by the interface character as well as by the defects present. The variations in experimental observations with chemical composition and size (as shortly discussed in the introduction and further elucidated in the next section) are a reflection hereof. Di Stefano et al. [25] performed the first detailed study of H trapping at the carbide/matrix interface using DFT calculations. They reported that interstitial sites at a perfect coherent interface $\{001\}_{Fe}/\{001\}_{TiC}$ correspond to binding energies of 31 kJ/mol (0.32 eV) while a C-vacancy or misfit dislocation at this interface resulted in higher binding energies of 44 kJ/mol (0.46 eV) and 47 kJ/mol (0.49 eV), respectively. The interstitial positions at the incoherent $\{011\}_{Fe}/\{001\}_{TiC}$ interface were found to be the weakest trapping sites, with a binding energy of 19 kJ/mol (0.2 eV), while the C-vacancy at this interface acted as a very strong trap with a binding energy of 87 kJ/mol (0.9 eV). Later, multiple DFT studies evaluated the H interactions at different sites related to the coherent carbide/matrix interfaces, visualized in Figure 3, for various transition metal carbides of the MC-type. An overview of these results is presented in Figure 4, together with results on the semi-coherent interface, i.e. containing misfit dislocations. Clearly, the C-vacancies at the interface (Vac_i) and second layer of the carbide (Vac_{L2}) provided the strongest trapping sites while interstitial positions at the coherent interface and in the strained Fe lattice were generally related to relatively low binding energies. Limited studies have been performed on the presence of misfit dislocations, but it can be concluded that these could also act as relatively strong trapping sites. When comparing the different carbides, one may conclude that the TiC provided the highest binding energy sites. However, the coherent interface related to the NbC seems to be slightly higher in binding energy than for the TiC. In conclusion, H trapping at the carbide interfaces is characterized by a wide variety of binding energies related to different sites, which are strongly influenced by the chemical composition of the carbide.

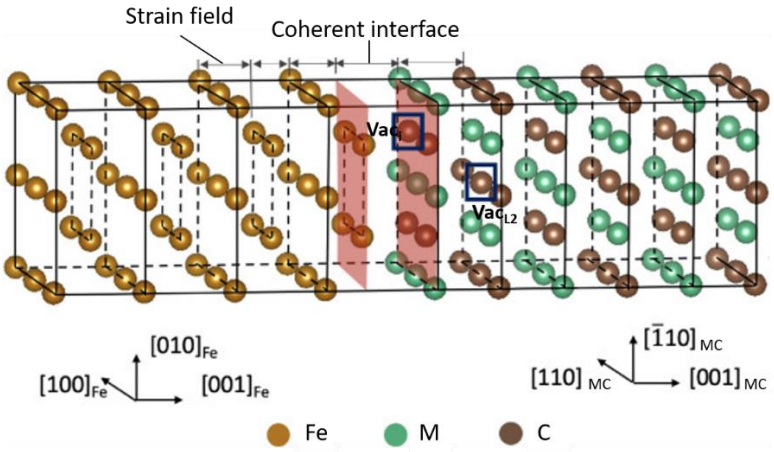

Figure 3: Schematic visualization of the different sites related to a coherent MC/Fe interface, adapted from Sagar et al. [34], published in International Journal of Hydrogen Energy (Elsevier), 2024. Vac_i and Vac_{L2} indicate a carbon vacancy at the interface (i) or in the second layer of the carbide (L2).

Moreover, steels often contain mixed carbides or mixed carbonitrides, which might affect the hydrogen interactions with these carbides. Therefore, Zhang et al. [38] and Hammer et al. [24] evaluated the effect of variations in chemical composition on the H binding energies. Zhang et al. [38] indicated that the presence of a Cr, W or Mo atom as a foreign substitutional atom in the carbide reduces the binding energy for all trapping sites associated with the interface, i.e. the interstitial positions at the interface as well as the C-vacancy sites. Hammer et al. [24] performed an extensive study on H trapping by mixed (Ti,V) carbonitrides, written as $Ti_yV_{1-y}C_xN_{1-x}$. They observed that the H binding energies to different trapping sites related to the carbide/matrix interface depends considerably on the local chemistry surrounding the H atom. They reported stronger H segregation at and near the interface of Ti- and C-rich precipitates while higher V and N contents showed a decreased segregation tendency. This was related to the substantially larger misfit strain for Ti-rich carbides. Similarly, C-vacancies at the coherent interface provided the highest binding energy of around 108 kJ/mol (1.12 eV) for TiC while increasing the N content and V content led to a nearly linear decrease of the binding energy, reaching 68 kJ/mol (0.7 eV) for TiN, 52 kJ/mol (0.54 eV) for VC, and 37 kJ/mol (0.38 eV) for VN. However, it was also noted that addition of V lowered the C-vacancy formation energy, potentially increasing the trap density. For the misfit dislocations, the highest binding energy was observed for TiN rather than TiC. Moreover, mixing of C and N resulted in slightly higher binding energies than predicted by linear extrapolation of the pure compounds. Alloying with V again resulted in a decrease of binding energy. However, V was also shown to decrease both misfit strain and chemical interface energy, which was related to an increase in the likelihood for precipitate nucleation, thus possibly leading to an increased trapping density. Consequently, they showed that the semi-coherent interfaces of $Ti_yV_{y-1}C_xN_{x-1}$ precipitates in steel matrix could provide a whole range of trapping sites, for which the density and binding energy is changed upon alloying.

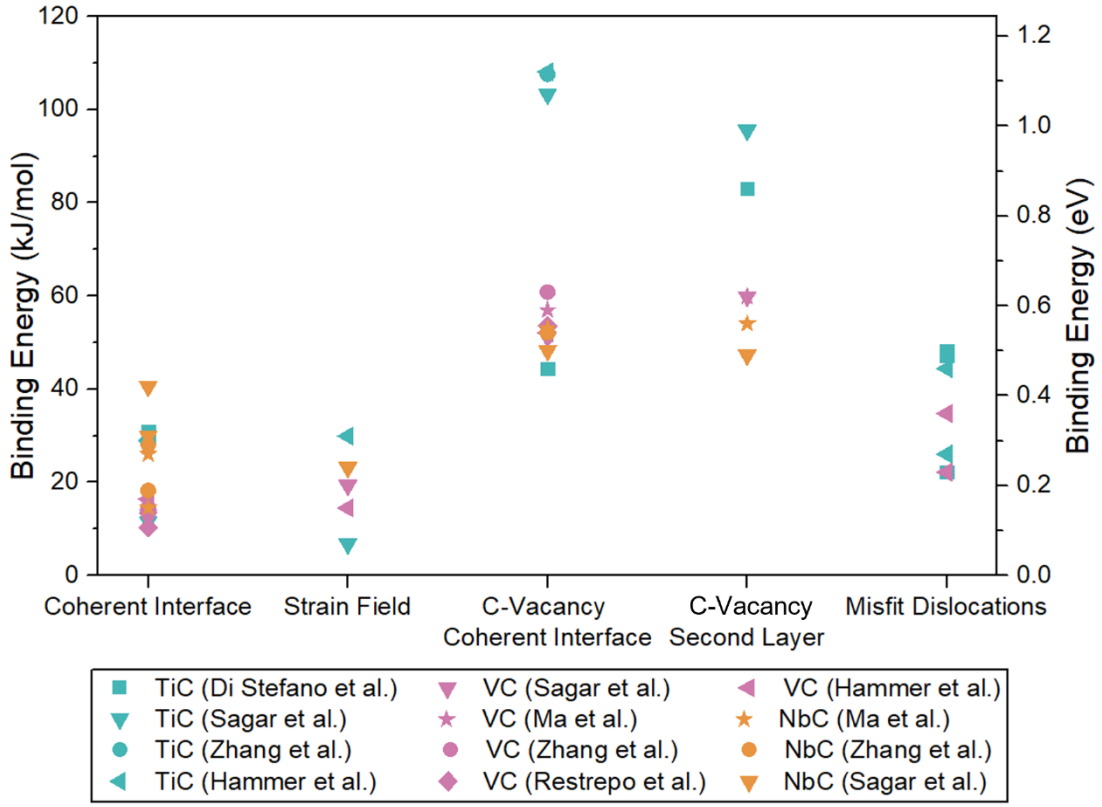

Figure 4: Overview of the binding energies related to different sites at the semi-coherent MC/Fe interface, calculated with DFT by Di Stefano et al. [25], Sagar et al. [34], Zhang et al. [38], Hammer et al. [24], Ma et al. [22], and Restrepo et al. [39].

3 Experimental characterization of the hydrogen-carbide interactions

While DFT calculations might provide important insights in the interactions of H with carbides, experimental characterization is crucial as well. The DFT calculations can be strongly affected by assumptions regarding initial configuration or computational details and hence might not always represent reality correctly. For example, the DFT study performed by Kawakami and Matsumiya [20] suggested H could not be trapped in cementite bulk due to high migration barriers. However, Chen et al. [31] visualized H trapping inside the cementite in pearlitic steels by APT. This was related to the presence of C-vacancies in the cementite together with a stress gradient, affecting the H migration and binding energies. Thus, experimental verification of the DFT results remains extremely important.

One of the standard methods to characterize H trapping by microstructural features includes thermal desorption spectroscopy (TDS), often combined with additional microstructural characterization. A vast amount of TDS-based studies on the H-carbide interactions in steels can be found in literature. However, only a selection of the more recent studies are discussed here. Also other techniques have been used to study H trapping at carbides. For instance, small angle neutron scattering (SANS) was used by Ohnuma et al. [28], demonstrating H trapping by small disc-shaped NbC, but did not allow for distinction between trapping at the interior or at the matrix/carbide interface. Malard et al. [29] also used SANS to study the H trapping by VC in twinning-induced plasticity steels and concluded that the H atoms were homogeneously distributed in the carbides rather than segregated at the carbide/matrix interface. However, it must be noted that these steels have an austenitic (FCC) steel matrix rather than a BCC steel matrix, which could strongly affect features such as the interface character or H migration and thus cannot simply be transferred to the ferritic steels. Moreover, this technique gives indirect

information on the trapping sites. Direct visualization of H trapping by carbides is of high importance to gain more certainty regarding the H distribution. Techniques such as secondary ion mass spectroscopy (SIMS), scanning Kelvin probe force microscopy (SKPFM), and atom probe tomography (APT) may be useful in this regard.

In the next sections, the experimental characterization of H interactions with Ti, V and Nb carbides by TDS and/or visualization techniques are discussed and related to the input obtained by DFT in order to obtain new insights. Afterwards, an overview of the different trapping energies (represented by E_B or E_a) of the different carbide-related trapping sites is provided as a summary under the form of a table.

3.1 Titanium carbides

Titanium carbides are well-known for their strong H trapping potential together with good precipitation strengthening, making them interesting features in the design of high-strength steels with improved HE resistance. Consequently, their interactions with H have been subject of many experimental studies, leading to a large range of reported E_a and/or E_B values.

Extensive TDS studies on the H trapping behavior after electrochemical charging at room temperature were performed by Wei et al. [26, 40] and Depover and Verbeken [8]. Both groups reported the presence of multiple trapping sites with E_a-values in the ranges of 40 kJ/mol to 50 kJ/mol (0.41-0.52 eV) and of 70 kJ/mol to 120 kJ/mol (0.72-1.24eV). Additionally, they both reported a strong influence of carbide size and correlated trapping to the carbide/matrix interfaces of the precipitated (semi-)coherent carbides. Wei and Tsuzaki [26] reported that the precipitated carbides were disc-like and oriented in the iron matrix according to the Baker-Nutting (B-N) orientation relationship (OR), with a broad (semi-)coherent $\{001\}_{Fe}/\{001\}_{TiC}$ interface and side interfaces which becomes incoherent upon carbide growth. They found that both the broad and side interface of the precipitated carbides could trap H after electrochemical charging but the corresponding de-trapping activation energy evolved differently with tempering temperature, as visualized in Figure 5. Moreover, the H concentration trapped at the broad interface was stated to be proportional to the interfacial area, while this was not the case for the H trapped at the side interfaces. An E_a of around 56 kJ/mol (0.58 eV) was reported for trapping at the broad interface, showing no influence of the tempering temperature. Based on the trapped H concentration, E_a, and link with carbide size, the misfit dislocations were identified as the responsible trapping features. The trapping at the side interface changed significantly with tempering temperature, which was related to the transition from (semi-)coherent to incoherent. For low tempering temperatures, i.e. small precipitates, the side interface acted like the broad interface and showed E_a values of around 56 kJ/mol (0.58 eV), related to the misfit dislocations. Upon increasing the tempering temperature, the dislocations at the side interface lose their individual character, which was reflected in a gradual increase of the trapping energy to 100 kJ/mol (1.0 eV), indicating a change of responsible trapping site. However, the amount of H, trapped after electrochemical charging, decreased, suggesting an increase in the barrier (E_t) to enter the corresponding trapping sites. Incoherent carbides were found to be unable to trap hydrogen after electrochemical charging but could trap hydrogen during processing. No clear interpretation was provided for these observations but it was suggested that the C-vacancies at the interior might play a role.

On the other hand, Depover and Verbeken [8] correlated the different trapping sites to carbides with different sizes, where the strongest trapping site (E_a>60 kJ/mol or 0.62 eV) was related to the interface between the semi-coherent carbides and the martensitic matrix while the other trapping sites were related to coherent carbides. By performing tempering for very long times (10h – 20h) they confirmed that the incoherent particles were unable to trap H from electrochemical charging. In order to obtain more insight in the trapping characteristics of the Fe-C-Ti alloys, Drexler et al. [41] used a numerical,

trap-diffusion integrated finite element model (FEM) for analysis of the TDS spectra obtained by Depover et al. [8]. They reported the presence of five different traps with binding energies of 15-20 kJ/mol (0.16-0.21 eV), 20-28 kJ/mol (0.21-0.29 eV), 55-60 kJ/mol (0.57-0.62 eV), 71-81 kJ/mol (0.74-0.84 eV), and 93-104 kJ/mol (0.97-1.14 eV). By evaluation of the trap density and comparison of the binding energies with the DFT results of Di Stefano et al. [25], they identified the responsible microstructural sites as:

(1) martensitic lath boundaries,
(2) coherent carbide/matrix interface,
(3) C-vacancies in the broad $\{001\}_{Fe}/\{001\}_{TiC}$ interface,
(4) C-vacancies at the incoherent $\{110\}_{Fe}/\{001\}_{TiC}$ interface,
(5) bulk C-vacancies in precipitates smaller than 20 nm.

While this interpretation is already closer related to the physical meaning behind the trapping, there is no reason for the disappearance of trapping by C-vacancies simply with increasing precipitate size. Possibly, the increase in carbide size was accompanied by a decrease of the C-vacancy concentration, leading to removal of the trapping sites or increased entry barrier. However, this was not experimentally confirmed.

Takahashi et al. [42] visualized the H trapping at fine precipitated TiC by use of APT. The precipitated TiC were reported to be present as disc-like particles following the B-N relation. APT showed deuterium (D) enrichment at the broad interfaces of the fine precipitated carbides rather than at the bulk of the carbides. The D atoms were observed homogenously along the broad surface. Therefore, the strain field was excluded as main trapping site. Additionally, the incoherent side interfaces of the precipitate were only considered weak trapping sites. Moreover, they found that precipitates smaller than 3 nm did not show any D segregation while larger precipitates were always decorated with D. Consequently, they identified the defects, e.g. misfit dislocations or C-vacancies, at the broad semi-coherent interface as the responsible trapping sites, in good agreement with the previously reported experimental observations and DFT calculations.

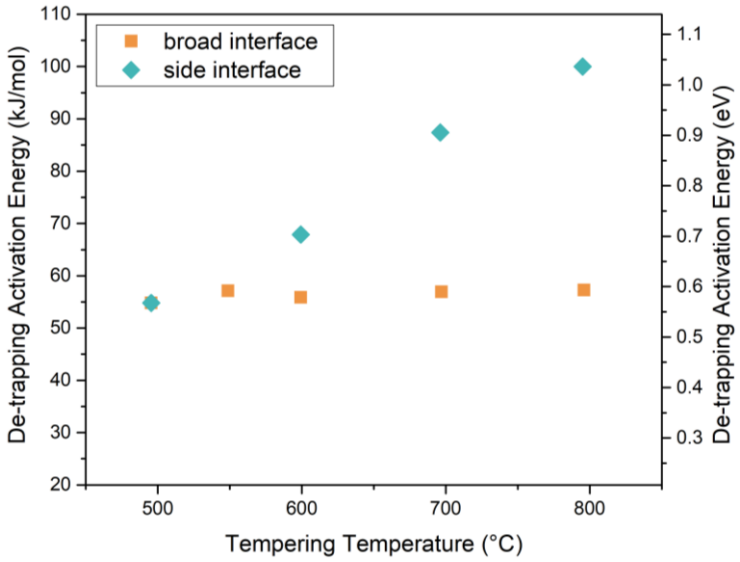

Figure 5: Change in de-trapping activation energy upon tempering temperature of different trapping sites related to precipitated carbides as determined by Wei and Tsuzaki [26].

Studies performed by Wei and Tsuzaki [26, 40, 43] and Perez Escobar et al. [27] indicated that charging of H at elevated temperatures from a gaseous atmosphere activated different trapping sites than electrochemical charging at room temperature. More specifically, incoherent carbides could not be

filled during electrochemical charging, but they could clearly trap H after gaseous charging at elevated temperatures. On the other hand, (semi-)coherent carbides/matrix interfaces did not trap H after gaseous charging. This was related to the high energy barrier present for entering of, and migration through the carbides, inhibiting uptake of H with low thermal energy, combined with the high binding energies related to the C-vacancies inside these carbides, leading to trapping at even very high temperatures of 500°C and above. As a result, the incoherent carbides were able to trap H when charged at elevated temperatures while electrochemical charging only resulted in H trapping by small, precipitated semi-coherent carbides. However, uncertainty still exists regarding the exact trapping mechanism of these carbides. Wei et al. [26, 40] reported a large range of de-trapping activation energies, from 68 kJ/mol to 137 kJ/mol (0.7 eV-1.42 eV), depending on austenitization and tempering temperature. This variation was suggested to be related to different trapping sites related the incoherent carbides. However, as the trapping sites are correlated to the C-vacancies in the titanium carbide bulk, one would not expect such strong variations in the binding energies based on the DFT results. Thus, the variations should rather be related to the migration energy of H through the carbides, which might be affected by factors such as C-vacancy concentration and network formation. On the other hand, Perez Escobar et al. [27] reported the presence of two or even three desorption peaks related to trapping by the incoherent carbides, all with similar de-trapping activation energies of around 140 kJ/mol to 150 kJ/mol (1.45-1.55 eV), depending on tempering/charging temperature, but with different pre-exponential factors. However, no physical interpretation behind the differences in pre-exponential factors was given.

Later studies, dedicated to the trapping from elevated gaseous H_2-containing atmospheres, were performed by Vandewalle et al. [44] and Boot et al. [33]. Vandewalle et al. [44] tempered martensitic generic Fe-C-Ti alloys, differing in undissolved carbide content, at 600°C in a dilute H_2 atmosphere and evaluated the corresponding H uptake. They indicated that the undissolved carbides provided the main trapping sites in these conditions while a minor contribution of the precipitated could not be excluded. TDS revealed one main desorption peak in the range of 500°C to 800°C. It was argued that trapping occurred mainly at the bulk C-vacancies and desorption was governed by migration of H through the carbides. Unfortunately, they could not obtain reliable de-trapping activation energies due to experimental variations. On the other hand, Boot et al. [33] observed multiple desorption peaks in the TDS spectra. Interestingly, the (semi-)coherent carbides were noted to trap H from the gaseous environment as well, in contrast to the observations of Vandewalle et al. [44]. This might be related to the gradual cooling down in the H_2 atmosphere in the experiments of Boot et al. [33] leading to additional charging at lower temperatures. As such, also trapping sites with lower binding energies could be filled. This is in good agreement with the results of Takahashi et al. [42] who used gaseous deuterium charging at 250°C-300°C and visualized trapping at the broad interface of the semi-coherent precipitates. However, Boot et al. [33] reported stronger trapping by the fine coherent carbides smaller than 5 nm than for the semi-coherent carbides, with corresponding E_a values of 96 kJ/mol (0.99 eV) and 42 kJ/mol (0.44 eV), respectively.

Interestingly, Boot et al. [33] were able to visualize the H trapping at the incoherent titanium carbides by use of the SIMS technique. While some of the carbides showed full H coverage, many contained a heterogeneous distribution, with H mainly present at the outer regions. Consequently, H was suggested to be trapped at the C-vacancies at the incoherent interface rather than in the bulk of the titanium carbides. Visualization of H trapping at Ti-based carbides was also performed by use of the SKPFM technique by Zhang et al. [45]. They analyzed the H trapping by incoherent precipitates in a martensitic HSLA steel. It was visualized that for some precipitates the incoherent interfaces trapped H while for others H was excluded from the interface and surrounding area, as can be seen in Figure 6. In order to reveal the underlying factors, focused ion beam was used to extract the precipitates of

interest for scanning transmission electron microscopy (STEM) investigation. Both precipitates were found to be of the Ti_2CS type and showed no OR, confirming their incoherent nature. However, electron energy loss spectroscopy (EELS) showed a higher concentration of C- and S-vacancies at the carbide/matrix interface of the carbide which trapped H, than at the one which excluded H. Hence, confirming the importance of the non-metal vacancies as H trapping sites. Moreover, the strain state in the martensitic matrix surrounding the precipitates was analyzed, showing a compressive strain field surrounding the precipitate excluding H at the area close to its interface, while the other precipitate was surrounded by a tensile strained matrix. Consequently, Zhang et al. [45] showed that both the presence of C- and/or S-vacancies at the precipitate interface and the strains surrounding the incoherent particles determined the H trapping behavior of the incoherent interface. However, due to the limited resolution, trapping at the fine (semi-)coherent carbides could not be studied by SKPFM.

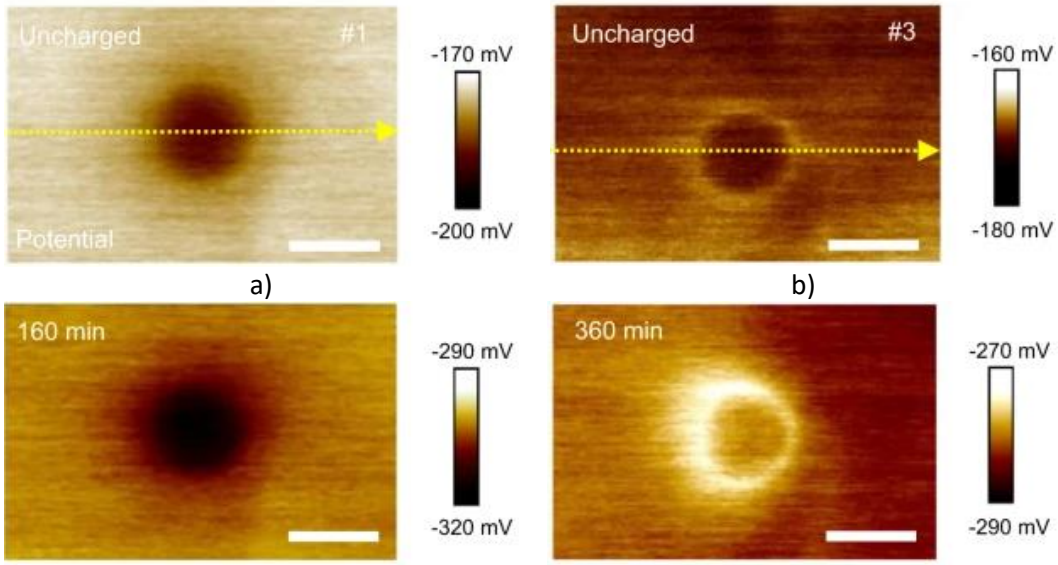

Figure 6: SKPFM visualization of two incoherent particles in the same steel, interacting very differently with hydrogen, adapted from Zhang et al. [45] published in Nature Communications (Springer Nature) 2022.

Lastly, some studies concerned the influence of the presence of other alloying elements on the H trapping behavior of the titanium carbides. Lin et al. [46] studied the H trapping in a dual precipitating (TiC and ε-copper) martensitic material and clearly observed an influence of the precipitation sequence. Co-precipitation was found to result in more and stronger trapping than sequential precipitation, which was related either to the presence of additional trapping sites due to impingement of co-precipitation or to the size restriction of the carbides resulting from this impingement. Jin et al. [47] studied the trapping by mixed (Ti,Mo) carbides in commercial medium C Cr-Mo steels. They found that fine precipitated (Ti,Mo) carbides with sizes between 1 nm and 5 nm and a Ti/Mo ratio of around 2 resulted in significant H uptake but the trapping was characterized by rather weak E_a (17-21 kJ/mol or 0.18-0.22 eV) compared to pure TiC [8, 26, 40]. Consequently, they suggested that partial replacement of Ti by Mo in the carbides resulted in a decrease of the de-trapping activation energy. This can be related to the DFT observations of Hammer et al. [24, 48], showing that H trapping by TiC is strongly affected by the presence of elements such as V and Mo. Lastly, Jin et al. [47] reported strong trapping (E_a=142 kJ/mol=1.47 eV) by the large, undissolved (Ti,Mo) carbides (with Ti/Mo ratio of around 5). However, these sites were shown to be inaccessible by electrochemical charging at room temperature similar to the pure TiC and hence were filled during processing.

3.2 Niobium carbides

Wei et al. [49] indicated that NbC could trap the most H of the three carbides; NbC, TiC and VC. This was related to the misfit dislocation density at the broad carbide/matrix interface of semi-coherent carbides. In another study [50], they mentioned that the trapping by NbC was associated to various sites related to the carbide, differing in binding energy. Interestingly, Wei et al. [49] also indicated that the undissolved NbC did not show strong H trapping from the tempering atmosphere, in contrast to the TiC. The latter observation could be related to the much lower binding energy of H to C-vacancies in the NbC structure compared to the TiC structure as determined by DFT (see Figure 2).

Wallaert et al. [51] studied the H trapping by NbC and NbN both upon electrochemical charging at room temperature and during gaseous charging at 800°C. They observed moderate trapping after electrochemical charging for the small (<30 nm) NbC with E_a values of 42 kJ/mol. Increasing tempering time resulted in the presence of both small and larger NbC and introduced an additional desorption peak with E_a = 48 kJ/mol (=0.50 eV). The gaseous charging was performed for much longer times than previous tempering steps, causing considerable carbide coarsening. A high temperature desorption peak appeared with activation energy of 63-68 kJ/mol. This peak was linked to trapping by bulk C-vacancies in the coarse NbC. This is in strong contrast to the observation of Wei et al. [49, 50]. The difference could be related to lower tempering/charging temperature applied by Wei et al. [49, 50], providing lower thermal energy, or the lower H_2 partial pressure during tempering, leading to lower H concentrations, as well as to differences in material conditions regarding chemical composition and prior austenitization, leading to potentially different carbide sizes or C-vacancy concentrations. Additionally, the DFT calculations did not support strong trapping by bulk C-vacancies in NbC. Such high trapping energies would rather be expected for the C-vacancies at the interface or in the outer carbide layers. However, Salehin et al. [36] reported a considerable increase in E_B with C-vacancy concentration, up to around 67.5 kJ/mol (0.7 eV). Consequently, the different trapping behavior at elevated temperatures might be related to different carbide structures. However, detailed carbide characterization by TEM and EELS would be necessary to confirm this hypothesis.

For the samples containing NbN, electrochemical charging revealed presence of two trapping sites related to these precipitates but with much lower E_a than for the carbides, i.e. 33 kJ/mol and 39 kJ/mol. Gaseous charging revealed a high temperature peak but with higher activation energy than for the carbides: 100 kJ/mol to 143 kJ/mol. The latter observation is in perfect agreement with the first principle calculations of Ma et al. [22], revealing a higher binding energy for the non-metal vacancy in NbN than for the NbC, i.e. 45 kJ/mol (0.47 eV) vs 20 kJ/mol (0.21 eV). However, trapping at non-metal vacancies at the (semi-)coherent interfaces was not reported to vary by going from NbC to NbN. The H binding energy at the tetrahedal sites in the strained Fe-lattice at the coherent interface were higher than for the NbN, i.e. 26 kJ/mol (0.27 eV) vs 11 kJ/mol (0.12 eV). However, these values are both significantly lower than the experimentally determined values. The size distribution of the NbN particles observed by Wallaert et al. [51] was also characterized by a significantly higher fraction of coarser particles, with length between 30 nm and 70 nm. Consequently, differences in coherency might have played an important role in the different interface trapping.

An extensive study on H trapping by NbC nano-precipitates in tempered martensitic steels was performed by Shi et al. [52] combining HRTEM, TDS, and DFT. Based on the HRTEM studies, they evaluated the precipitate size distribution for different tempering times along with carbide interfacial character. The precipitates contained semi-coherent interfaces, aligned according to the Kurdjumov-Sachs (K-S) OR rather than the B-N OR, implying a semi-coherent rather than coherent character. Moreover, they reported the presence of two sets of misfit dislocations and a high misfit dislocation density. DFT calculations were performed to evaluate the trapping at the coherent interface with the

B-N OR, with and without C-vacancies, and at the semi-coherent interface with K-S OR. It was concluded that the semi-coherent interface corresponded to a very high binding energy of around 77.2 kJ/mol (0.80 eV). Additionally, they stated that the stable H position most likely corresponded to the misfit dislocation. Finally, TDS was performed revealing two desorption peaks, one with low E_a of 20 kJ/mol (0.21 eV) and one with high E_a of 82 kJ/mol (0.85 eV). While the first was related to the martensitic matrix (dislocations, grain boundaries etc.), the E_a of the second peak agreed with the binding energy for the misfit dislocations at semi-coherent interface calculated by DFT. Moreover, the trapping density decreased with tempering time, corresponding to coarsening of the NbC precipitates. Hence, using DFT, advanced microstructural characterization, and TDS, as complementary techniques, Shi et al. [52] were able to identify the misfit dislocations at the semi-coherent interfaces of NbC as the irreversible H trapping site.

Direct visualization of H trapping at NbC by APT was performed by Chen et al. [53] and Samanta et al. [32], as shown in Figure 7. While Chen et al. [52] observed mainly trapping at the NbC/matrix interface, Samanta et al. [32] could visualize H trapping at the carbide interior. However, it must be noted that the NbC studied by Chen et al. [53] were reported to be quite large and incoherent while Samanta et al. [32] reported the presence of small, finely dispersed NbC following the B-N OR. Moreover, the Nb/C ratio in the chemical composition was very different for both steels, which could indicate strong differences in C-vacancy concentration and as such differences in diffusion barriers and binding energies. Indeed, the atomic Nb/C ratio in the steel investigated by Chen et al. [53] was very low (around 0.03), while the material investigated by Samanta et al. [32] contained a rather high Nb/C ratio of 1.75. Therefore, the carbides in the steel of Samanta et al. [32] could be expected to contain a considerable amount of C-vacancies in the carbides while the carbides studied by Chen et al. [53] were considerably less likely to contain C-vacancies. Similarly, the materials studied by Shi et al. [52] contained a relatively low Nb/C (around 0.1) indicating abundance of C and thus probably limited amount of C-vacancies. Consequently, the difference in C-vacancy concentration could also be strongly involved in the different trapping behavior in addition to the carbide size.

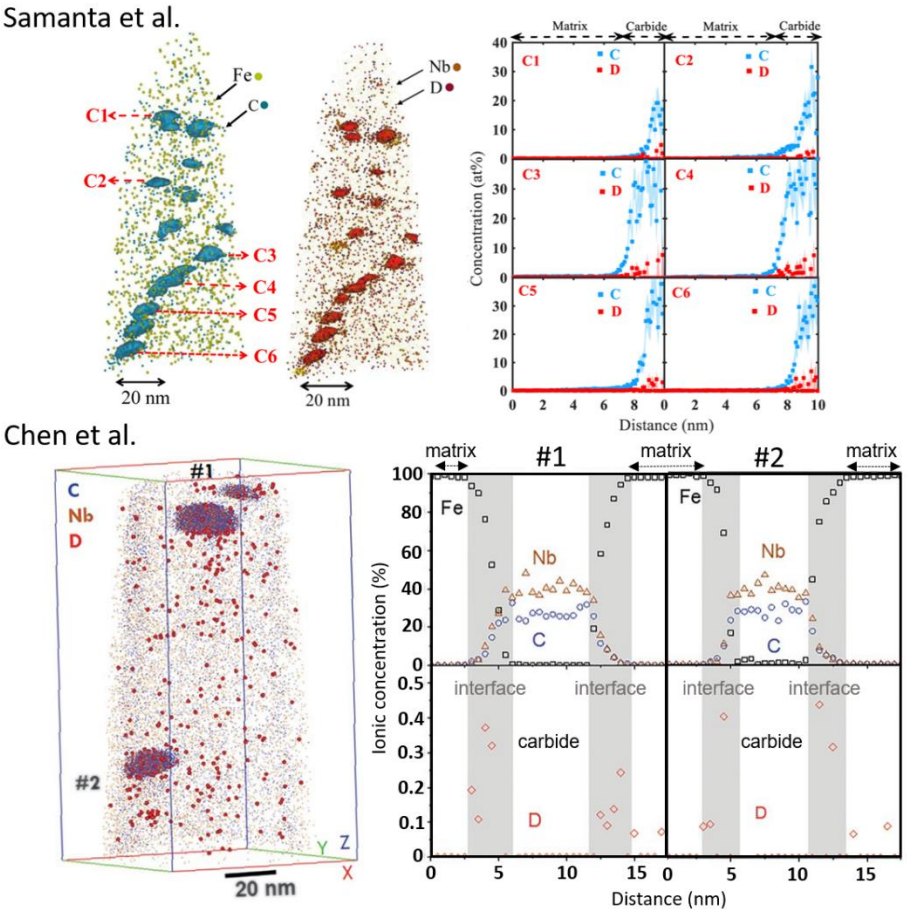

Figure 7: Visualization of deuterium (D) distribution at NbC by APT, as observed by Samanta et al. [32] (adapted with permission from [32], Copy right 2023, Elsevier) and Chen et al. [53] (adapted with permission from [55], Copyright 2020, The American Association for the Advancement of Science). While Samanta et al. [32] observed mainly trapping at interior of the NbC, Chen et al. [53] reported trapping at the carbide/matrix interfaces.

3.3 Vanadium carbides

The last NaCl-type carbide often considered in terms of improving strength and HE, are the vanadium carbides. While, these carbides have been noted to provide weaker trapping compared to the other two, vanadium carbides are especially interesting as their size distribution is easier to control, thanks to their higher solubility. Depover and Verbeken [12] evaluated the H trapping in tempered martensitic steels, where the C and V content were varied to maintain a V/C ratio of around 1.34, close to the V_4C_3 ratio. TDS showed clear influence of the vanadium carbides on the trapping behavior. Deconvolution of the TDS spectra indicated the presence of four different trapping sites with E_a-values of around 30 kJ/mol (0.31 eV), 52 kJ/mol (0.54 eV), 57 kJ/mol (0.59 eV), and 65 kJ/mol (0.67 eV). The first one was related to the martensitic matrix while the three with higher E_a-values were related to trapping by the carbides. By varying tempering time and evaluating the resulting changes in the TDS spectra and carbide size distribution, trapping was assumed to occur mainly at the carbide/matrix interface of the semi-coherent carbides with sizes below 20 nm. The strongest trapping site was related to the smallest carbides with sizes below 5 nm. Trapping by bulk C-vacancies was assumed to contribute to the second and third desorption peak. Carbides with sizes above 20 nm were considered to not play a major role in the H trapping. This was related to a change in E_B and E_t due to transition of the carbide/matrix interface to an incoherent character. Similarly as for the case of TiC, Drexler et al. [54] used a trap-diffusion integrated FEM to evaluate the TDS spectra of Depover and Verbeken [12]. They reported four different trapping sites related to the vanadium carbides. Each site was characterized by its

binding energy, being 32 kJ/mol (0.34 eV), 58 kJ/mol (0.60 eV), 73 kJ/mol (0.76 eV) and 92 kJ/mol (0.95 eV), on average. Additionally, the use of the model-based evaluation of the spectra allowed determination of the respective trapping densities. Combining these findings together with information obtained by experimental characterization of the underlying microstructures they identified the trapping sites as the coherent $\{001\}_{Fe}/\{001\}_{VC}$ interface, C-vacancies at the semi-coherent $\{001\}_{Fe}/\{001\}_{VC}$ interface, C-vacancies at the incoherent $\{011\}_{Fe}/\{001\}_{VC}$ interface and bulk C-vacancies, respectively. Interestingly, similar trapping sites and corresponding energies were found as for the TiC, even though DFT calculations generally predicted lower binding energies for the vanadium carbides than for titanium carbides. Even trapping by bulk C-vacancies with a high binding energy was reported for the vanadium carbides by Drexler et al. [54]. As mentioned previously, prolonging tempering from 1h to 2h resulted in the absence of this trap. As this corresponded to the disappearance of the smallest carbides (with radius < 5 nm), it was believed that only the C-vacancies in these very small, coherent carbides could be occupied. However, no in-depth explanation was given for this observation. Based on the TEM characterization, the carbides were considered to be V_4C_3 rather than VC. Hence, relatively large binding energies can be expected for the bulk C-vacancies. Even the value of 92 kJ/mol (0.95 eV) obtained by Drexler et al. [54] may seem to low considering the binding energies obtained by DFT calculations. Moreover, bulk trapping would require considerable H diffusion through the carbide lattice. Huang et al. [37] reported an activation energy of 204.5 kJ/mol (2.12 eV) for H migration in the V_4C_3 carbides. Consequently, even for very small carbides of 5 nm, one might expect considerably higher E_a values for de-trapping from bulk C-vacancies. On the other hand, direct jumps from one C-vacancy to another corresponded to migration energies of 93 kJ/mol (0.96 eV), which is close to the values obtained by Drexler et al. [54]. However, it must be noted that the latter represent E_B-values based on assumption of H desorption controlled by diffusion through the iron bulk, while local equilibrium is maintained between single trapping sites and the iron lattice. Consequently, this model might be less suitable to describe the complex de-trapping at bulk C-vacancies which require H diffusion through the carbides. Regarding the trapping at the interface, uncertainties exists as well. Unfortunately, very little DFT studies have been performed on the trapping at the interface of the V_4C_3 carbides with iron matrix. However, using the values of the VC-type of carbides, one might identify the first carbide-related peak as the interstitial sites at the perfect coherent interface and in the strained iron layers, while the second and third peaks could be related to the C-vacancies at the interface or to misfit dislocations. However, additional DFT calculations on different types of interfaces between vanadium carbides and iron are required to obtain more insight.

Lee et al. [10] evaluated the influence of V addition on H trapping and HE characteristics of a tempered martensitic steel with a fixed C content of 0.6 wt%. They observed that increasing the V content enhanced the H uptake after electrochemical charging, which was attributed to the trapping by vanadium carbides. Kissinger analysis revealed an E_a of around 27.4 kJ/mol (0.284 eV) for the 0.2 wt% V containing steel while for the V-free steel the E_a was determined to be only 14.1 kJ/mol (0.146 eV). Thus, the vanadium carbides clearly increased the de-trapping activation energy but the reported values were considerably lower than the values obtained by Depover and Verbeken [12]. In order to evaluate the effect of undissolved vs. precipitated carbides, the austenitization temperature was increased, which resulted in a strong increase of H uptake together with a shift of the peak temperature, indicating an increase in both trapping density and trapping strength. By comparison of the TDS curves of the different steels, they concluded that for 0.2 wt% V and 0.5 wt% V the main trapping sites corresponded to the broad {001} surface of the precipitated, plate-like V_4C_3 carbides, while the additional trapping observed in 1.0 wt% V was attributed to the broad {100} surface of the cuboidal V_6C_5 undissolved carbides together with the large carbides containing high concentration of V. However, no characterization of the carbide structures, e.g. by selected area electron diffraction

(SAED) or EELS, was reported. Consequently, uncertainty might exist regarding the exact nature of the vanadium carbides present. When comparing their observations with results from DFT calculations, the observed E_a-value is in good agreement with trapping by the coherent VC/Fe interface and by the strained iron layers close to the interface. Also binding energies in a similar range were observed for the C-vacancies in C-rich carbides such as the V_6C_5 and V_8C_7 structures, which would confirm the assignment of trapping to V_6C_5 carbides in the case of the 1.0 wt% V alloy. Trapping by C-vacancies at the VC/Fe interface seems rather unlikely due to the much higher binding energies reported by DFT and other experimental studies [12, 54]. However, it must be noted that only one single trapping site was considered by Lee et al. [10], even though the spectra were relatively broad and showed indications of high temperature shoulders. The numerical study of Drexler et al. [55] showed that incorrect deconvolution could lead to an underestimation of the de-trapping energies, especially in the case of overlapping peaks.

As the interface is generally reported as the most important trapping site, one might question the influence of the iron matrix. Analysis of the trapping behavior of VC in ferritic steels was done by Turk et al. [56]. They compared two steels with similar VC volume fraction but different carbide sizes. They established a correlation between trapping density and effective interface area, hence indicating that trapping mainly occurred at the coherent interfaces, similar for the martensitic materials. However, they also reported rather low H contents trapped by the VC compared to the uptake reported in martensitic steels [10, 12]. Therefore, they stated that the presence of dislocations in the matrix might have an influence on the H trapping by the carbide/matrix interfaces as well.

A systematic study on the H trapping at VC performed by Takahashi et al. [57] combined TDS and APT together with HRTEM to study the hydrogen trapping at fine vanadium carbides in under-, peak- and over-aged steels. They showed that while little H was introduced in the under-aged samples, strong trapping was present in the peak- and over-aged samples, with E_a around 60 kJ/mol (0.62 eV). Conversely, activation energies of around 25 kJ/mol (0.26 eV) were observed for the trapping in under-aged samples. Additionally, APT showed no enrichment around the perfectly coherent VC in the under-aged samples while strong segregation at the broad {001} interface of the VC platelets in the peak-aged samples was observed, as visualized in Figure 8. Based on HRTEM investigation and comparison of dislocation and trapping density, the misfit dislocations were ruled out as potential trapping site. Instead, chemical analysis showed that the change from VC to V_4C_3 coincided with increased trapping capacity and hence, the C-vacancies at the carbide/matrix interface were considered as the responsible trapping sites. On the other hand, APT observations by Chen et al. [30] clearly revealed deuterium trapping throughout the bulk of mixed (V,Mo)-carbides, as shown in Figure 9. In order to elucidate these different observations, the experimental details regarding chemical composition, carbide size and charging procedure in the two studies are compared, as presented in Table 2. Both authors reported the presence of fine precipitates. Interestingly, the chemical composition reported by Takahashi et al. [57] showed a higher V/C ratio than the one reported by Chen et al. [30], which would suggest potentially higher C-vacancy concentration and thus lower H migration barriers in the carbide. Additionally, charging by Takahashi et al. [57] was done from a pure deuterium gas atmosphere at 200°C-300°C, implying higher thermal energy of the D atoms than for the electrochemically charged samples of Chen et al. [30]. Based on these observations one might expect higher probability of bulk trapping for the samples of Takahashi et al. [57] than for Chen et al. [30], opposite to the experimental observations. However, it must be noted that the bulk trapping observed by Chen et al. [30] stems from a rigorous statistical analysis, revealing the D distribution over the normalized carbide size of more than 100 precipitates. While, the interface trapping reported by Takahashi et al. [57] was based on the observation of D at the broad interface but the limited thickness of the samples might have complicated the distinction between interface and bulk trapping. On the other hand, the presence of

Mo in the V-based carbides as studied by Chen et al. [30] might promote bulk trapping over interface trapping, e.g. by alteration of the migration barriers or the C-vacancy formation energy.

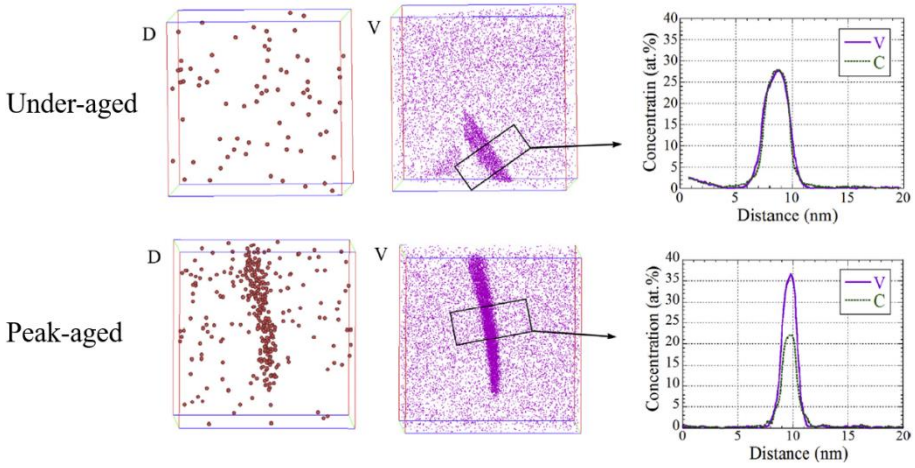

Figure 8: APT observation of deuterium trapping at vanadium carbides by Takahashi et al. [57]. The carbides in peak-aged samples, strongly decorated with deuterium (D), were characterized by high concentration of C-vacancies. On the other hand, carbides in under-aged samples, exhibiting nearly perfect stoichiometry, showed no D segregation, thus confirming the trapping action of the interface C-vacancies. Adapted with permission from [57], Copyright 2018, Acta Materialia Inc. Published by Elsivier Ltd.

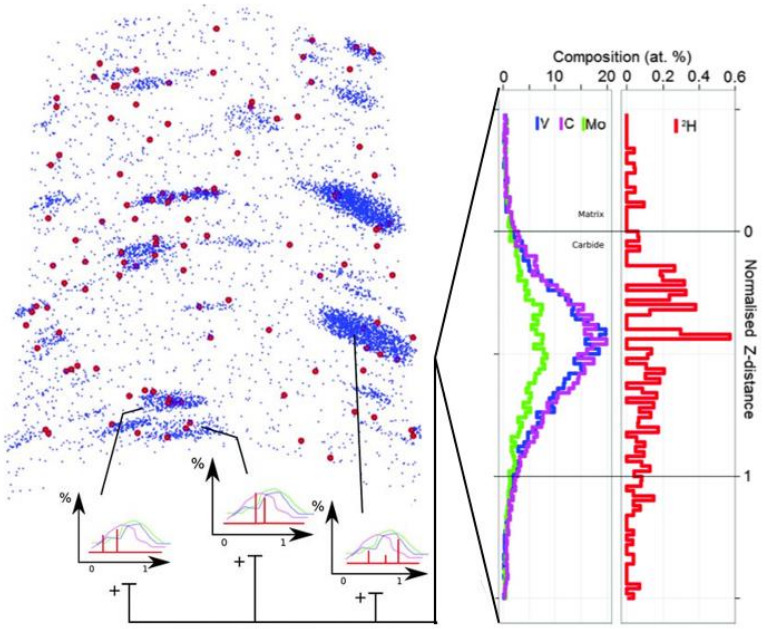

Figure 9: Visualization of D distribution at (Mo,V) carbides after electrochemical charging as observed by Chen et al. [30] with APT. A superimposition of the elemental distribution over the normalized z distance of the carbide is shown in the right, indicating bulk trapping rather than interfacial trapping. Reprinted with permission from [30], Copyright 2017, The American Association for the Advancement of Science.

Table 2: Differences between experimental APT studies of Takahashi et al. [57, 58] and Chen et al. [30].

	Takahashi et al. [57, 58]	**Chen et al. [30]**
Observations	trapping at broad $\{001\}_{VC}$ interface of semi-coherent carbides (>30nm in length)	trapping throughout the bulk of mixed (V,Mo) carbides
Composition (wt%)	Fe-0.060C-0.10Mn-3.0Al-0.50V-0.0014 N	Fe-0.096C-1.6Mn-0.026Si-0.51Mo0.25V-0.05Al-0.056Nb
At. V/C Ratio	1.96	0.61
Carbide size	10-60 nm	"nanoscaled"
OR	Baker-Nutting	/
Charging procedure	D_2 gas at 200°C-300°C	RT electrochemical charging

Finally, questions may arise regarding the trapping capacity from elevated temperatures by the bulk C-vacancies, similar as what was observed for the TiC. Wei et al. [49] reported that the incoherent vanadium carbides could not trap any H from the gaseous tempering environment in contrast to TiC. Similarly, Vandewalle et al. [59] reported the absence of a high temperature peak in the TDS spectrum of Fe-C-V alloys, tempered at 600°C in a dilute H_2 atmosphere. However, they mentioned the presence of a small desorption peak at 150°C to 200°C related to undissolved vanadium carbides. This is in strong contrast to the observations of Boot et al. [33], who reported significant, irreversible H trapping by vanadium carbides from pure H_2 atmospheres at elevated temperatures. Interestingly, the desorption peak appeared at high temperatures but slightly lower than compared to the titanium carbides, indicating slightly weaker trapping, which is in good agreement with the DFT results. SIMS investigation even visualized the H trapping at the large incoherent vanadium carbides, showing a homogeneous distribution over the entire carbides. Consequently, the high temperature desorption peak could be related to trapping at the bulk C-vacancies inside the incoherent vanadium carbides. The absence of strong trapping by the incoherent carbides in the studies of Vandewalle et al. [59] and Wei et al. [49] might be related to a difference in chemical composition, leading to lower binding energies as shown by DFT (see Table 1) or to a lower volume of undissolved carbides. However, more detailed characterization of the carbide sizes and structures would be necessary to confirm this.

Table 3: Overview of the reported trapping sites and their corresponding trapping energies (E_a or E_B, indicated as ^{A} or ^{B}, respectively) energies related to carbides. While the first column specifies the trapping site as reported in the original source, the last column provides additional comments regarding the assignation or reported energies.

Trapping site	**Trapping energy**		**Method**	**Source**	**Comments**
	(kJ/mol)	**(eV)**			
Titanium carbides					
Coherency strain field	18 ± 12^B	0.19 ± 0.12^B	DFT	[24,34]	
Incoherent $\{110\}_{Fe}/\{001\}_{TiC}$ side interface	19^B	0.20^B	DFT	[25]	
Coherent $\{001\}_{Fe}/\{001\}_{TiC}$ interface	24 ± 8^B	0.25 ± 0.09^B	DFT	[24,25, 34,38]	

Coherent $\{001\}_{Fe}/\{001\}_{TiC}$ interface	19±2[A]	0.20±0.02[A]	TDS	[47]	mixed (Ti,Mo) carbides with Ti/Mo = 2
Coherent $\{001\}_{Fe}/\{001\}_{TiC}$ interface	24±4[B]	0.25±0.04[B]	TDS	[41,54]	
Misfit dislocation at semi-coherent $\{001\}_{Fe}/\{001\}_{TiC}$ interface	41±9[B]	0.43±0.09[B]	DFT	[24,25]	
Misfit dislocation at semi-coherent $\{001\}_{Fe}/\{001\}_{TiC}$ interface	55±3[A]	0.57±0.03[A]	TDS	[26,40]	
Semi-coherent carbides	42[A]	0.44[A]	TDS	[33]	probably related to misfit dislocations
Coherent interface	47±5[A]	0.49±0.05[A]	TDS	[8]	Might be related to misfit dislocations rather than coherent interface
C-vacancies in (semi-) coherent $\{001\}_{Fe}/\{001\}_{TiC}$ interface	90±22[B]	0.94±0.23[B]	DFT	[24,25, 34,38]	Large variation due to low value reported by Di Stefano et al. [25]
C-vacancies in (semi-) coherent $\{001\}_{Fe}/\{001\}_{TiC}$ interface	58±3[B]	0.60±0.03[B]	TDS	[41,54]	Might also be related to misfit dislocations instead
C-vacancies at incoherent $\{110\}_{Fe}/\{001\}_{TiC}$ side interface	87[B]	0.9[B]	DFT	[25]	
Semi-coherent interface	83±25[A]	0.86±0.26[A]	TDS	[8]	Might be related to c-vacancies at interface of semi-coherent carbides (also strong influence of C and Ti content)
C-vacancies at incoherent $\{110\}_{Fe}/\{001\}_{TiC}$ side interface	76±5[B]	0.79±0.05[B]	TDS	[41,54]	
Incoherent $\{110\}_{Fe}/\{001\}_{TiC}$ side interface of precipitated carbides	85±13[A]	0.88±0.14[A]	TDS	[26,40]	Probably related to the C-vacancies at the side interface (strong influence of tempering temperature)
Coherent carbides (< 5nm)	96[A]	0.99[A]	TDS	[33]	Probably related to the C-vacancies
Bulk C-vacancy in TiC	115±10[B]	1.19±0.11[B]	DFT	[18,24, 25,34-36]	
Bulk C-vacancy in coherent TiC (< 20 nm)	103±9[A]	1.07±0.09[A]	TDS	[41,54]	Due to high entering barriers in TiC, must be related to interface C-vacancies or C-vacancies connected to surface via continuous vacancy network
C-vacancy in incoherent carbides	68-137[A]	0.70-1.42[A]	TDS	[26,40, 43]	H introduction during tempering + strong influence of tempering temperature

C-vacancy in incoherent carbides	146±5[A]	1.51±0.05[A]	TDS	[27]	Gaseous H charging
C-vacancy in incoherent carbides	142[A]	1.47[A]	TDS	[47]	Undissolved mixed (Ti,Mo) carbides with Ti/Mo ratio of 5 (H originated from processing)
Niobium carbides					
Coherency strain field	23[B]	0.24[B]	DFT	[34]	
Coherent $\{001\}_{NbC}/\{001\}_{Fe}$ interface	26±8[B]	0.27±0.09[B]	DFT	[22,34,38]	
C-vacancy at coherent $\{001\}_{NbC}/\{001\}_{Fe}$ interface	51[B]	0.53[B]	DFT	[22,34,38]	
(semi-)coherent NbC (<30 nm)	41±2[A]	0.42±0.02[A]	TDS	[51]	Might be related to misfit dislocations at B-N carbides but no DFT values
Semi-coherent to incoherent NbC (30 nm - 150 nm)	48[A]	0.50[A]	TDS	[51]	Might be related to C-vacancies at interface
Misfit dislocation at semi-coherent $\{1\bar{1}\bar{1}\}_{NbC}/\{001\}_{Fe}$ interface	77[B]	0.80[B]	DFT	[52]	
Misfit dislocation at semi-coherent $\{1\bar{1}\bar{1}\}_{NbC}/\{001\}_{Fe}$ interface	82[A]	0.85[A]	TDS	[52]	
Bulk C-vacancy in NbC	22±3[B]	0.23±0.03[B]	DFT	[22,34,36]	
Bulk C-vacancy in Nb_3C_2	68[B]	0.70[B]	DFT	[36]	
C-vacancy in incoherent carbides	66±3[A]	0.68±0.03[A]	TDS	[51]	Might be related to metal-rich incoherent NbC
Vanadium Carbides					
Coherency strain field	17[B]	0.18[B]	DFT	[24,34]	
Coherent $\{001\}_{VC}/\{001\}_{Fe}$ interface	12±2[B]	0.13±0.02[B]	DFT	[22,24,34,38,39]	
Misfit dislocation at $\{001\}_{VC}/\{001\}_{Fe}$ interface	28±6[B]	0.30±0.07[B]	DFT	[24]	
Coherent $\{001\}_{VC}/\{001\}_{Fe}$ interface	32±4 [B]	0.34±0.04 [B]	TDS	[54]	quite high compared to DFT value, perhaps related to misfit dislocation
coherent carbides	25[A]	0.26[A]	TDS	[57]	
(semi-)coherent carbides	26[A]	0.27[A]	TDS	[56]	

semi-coherent carbides	27[A]	0.28[A]	TDS	[10]	Value obtained by considering only one trapping site while being relatively broad
C-vacancy at (semi-)coherent $\{001\}_{VC}/\{001\}_{Fe}$ interface	55±4[B]	0.57±0.04[B]	DFT	[22,24, 34,38, 39]	
C-vacancy at (semi-)coherent $\{001\}_{VC}/\{001\}_{Fe}$ interface	58±2[B]	0.6±0.02[B]	TDS	[54]	
C-vacancy at semi-coherent $\{001\}_{VC}/\{001\}_{Fe}$ interface	60[A]	0.62[A]	TDS	[57]	
Coherent carbides (< 5nm)	65±2[A]	0.67±0.02[A]	TDS	[12]	Might be related to C-vacancies in coherent carbides
Semi-coherent carbides (5-20nm)	55±2[A]	0.56±0.02[A]	TDS	[12]	Might be related to C-vacancies in semi-coherent interface
C-vacancies at incoherent $\{110\}_{Fe}/\{001\}_{VC}$ side interface	73±4 [B]	0.76±0.04[B]	TDS	[54]	Was based on DFT value for TiC but no DFT studies on VC
Bulk C-vacancy in VC	25±7[B]	0.26±0.07[B]	DFT	[22,24, 34, 36]	
Bulk C-vacancy in V_4C_3	125±9[B]	1.29±0.09[B]	DFT	[37,18]	
Bulk C-vacancy in coherent V_4C_3 (< 5nm)	92±2[B]	0.95±0.02[B]	TDS	[54]	might rather be related to second or third layer C-vacancies or connected C-vacancy network

4 Conclusions and future outlook

The interactions of hydrogen with carbides in steels may strongly affect the hydrogen distribution in the steel and as such have an impact on the HE behavior. Therefore, study of these interactions is relevant in the search for more HE resistant materials. However, many different trapping sites can be related to the carbides, i.e. interstitial sites at the coherent and incoherent interface or in the strained steel matrix, defects at the interface, such as C-vacancies and misfit dislocations, or defects in the bulk, leading to a large range of binding energies. Analysis of DFT studies, reported in literature, indicated that defects play a primary role in the trapping by the carbides since the highest binding energies were associated to defected sites. For the TiC, the C-vacancy at the bulk was reported as the strongest trapping site, while for the NbC and VC the C-vacancies at the coherent interface could be considered as the strongest ones. Also the trapping barrier, i.e. the accessibility of the various trapping sites, varied considerably for the different trapping sites. While the interface related trapping sites could generally be considered easily accessible, high trapping barriers could exist for the C-vacancies in the bulk. Moreover, the trapping characteristics showed strong dependency on the local chemical environment or carbide crystal structure. Consequently, full understanding of the hydrogen-carbide interactions requires not only information on the trapping energies and densities present in the steels, which can experimentally be provided by TDS, but it also needs detailed characterization of the carbide structures. Additionally, direct visualization techniques such as APT, SIMS and SKPFM might enhance the understanding on the hydrogen distribution at the carbides. Due to lower resolution, SIMS and

SKPFM could only provide information on the trapping by larger and thus incoherent carbides. While, APT was able to investigate the trapping even at fine nano-scale coherent and semi-coherent precipitates. However, drawback of the latter technique, besides the difficult sample preparation, involves the small observation volume, which might raise questions regarding statistics and reproducibility. Some discrepancies in experimental observations reported in literature could be elucidated by comparison of the chemical composition, carbide size or charging procedure in addition to comparison with theoretical input from DFT. However, for some studies no straightforward reason behind the different behavior could be found. Consequently, this review study strongly indicated the importance of detailed microstructural characterization of the carbides by different techniques complementary to the hydrogen trapping investigation. Additionally, some interesting subjects for future DFT studies regarding the hydrogen-carbide interactions were suggested in order to deepen the understanding of the hydrogen trapping action of the carbides.

Acknowledgements

The authors would like to acknowledge the doctoral fellowship (grant 11F6522N) and project funding (grant G069721N) of the Research Foundation – Flanders (FWO), together with the Special Research Fund (BOF), UGent (grants BOF15/BAS/062, BOF/GOA/026, and BOF20/BAS/121), for support.

References

[1] Depover T, Pérez Escobar D, Wallaert E, Zermout Z, Verbeken K. Effect of hydrogen charging on the mechanical properties of advanced high strength steels. International Journal of Hydrogen Energy. 2014;39:4647-56.
[2] Depover T, Laureys A, Perez Escobar D, Van den Eeckhout E, Wallaert E, Verbeken K. Understanding the Interaction between a Steel Microstructure and Hydrogen. Materials (Basel). 2018;11.
[3] Lee J, Lee T, Mun D-J, Bae CM, Lee CS. Comparative study on the effects of Cr, V, and Mo carbides for hydrogen-embrittlement resistance of tempered martensitic steel. Scientific Reports. 2019;9:5219.
[4] Peral LB, Fernández-Pariente I, Colombo C, Rodríguez C, Belzunce J. The Positive Role of Nanometric Molybdenum–Vanadium Carbides in Mitigating Hydrogen Embrittlement in Structural Steels. Materials2021.
[5] Depover T, Monbaliu O, Wallaert E, Verbeken K. Effect of Ti, Mo and Cr based precipitates on the hydrogen trapping and embrittlement of Fe–C–X Q&T alloys. International Journal of Hydrogen Energy. 2015;40:16977-84.
[6] Kim H-J, Jeon S-H, Yang W-S, Yoo B-G, Chung Y-D, Ha H-Y, et al. Effects of titanium content on hydrogen embrittlement susceptibility of hot-stamped boron steels. Journal of Alloys and Compounds. 2018;735:2067-80.
[7] Nagao A, Martin ML, Dadfarnia M, Sofronis P, Robertson IM. The effect of nanosized (Ti,Mo)C precipitates on hydrogen embrittlement of tempered lath martensitic steel. Acta Materialia. 2014;74:244-54.
[8] Depover T, Verbeken K. The effect of TiC on the hydrogen induced ductility loss and trapping behavior of Fe-C-Ti alloys. Corrosion Science. 2016;112:308-26.
[9] dos Santos TAA, de Lima MM, dos Santos DS, Buono VTL. Effect of nano Nb and V carbides on the hydrogen interaction in tempered martensitic steels. International Journal of Hydrogen Energy. 2022;47:1358-70.
[10] Lee J, Lee T, Kwon YJ, Mun D-J, Yoo J-Y, Lee CS. Effects of vanadium carbides on hydrogen embrittlement of tempered martensitic steel. Metals and Materials International. 2016;22:364-72.
[11] Seo HJ, Kim JN, Jo JW, Lee CS. Effect of tempering duration on hydrogen embrittlement of vanadium-added tempered martensitic steel. International Journal of Hydrogen Energy. 2021;46:19670-81.

[12] Depover T, Verbeken K. Evaluation of the effect of V_4C_3 precipitates on the hydrogen induced mechanical degradation in Fe-C-V alloys. Materials Science and Engineering: A. 2016;675:299-313.
[13] Depover T, Verbeken K. The detrimental effect of hydrogen at dislocations on the hydrogen embrittlement susceptibility of Fe-C-X alloys: An experimental proof of the HELP mechanism. International Journal of Hydrogen Energy. 2018;43:3050-61.
[14] Dadfarnia M, Sofronis P, Neeraj T. Hydrogen interaction with multiple traps: Can it be used to mitigate embrittlement? International Journal of Hydrogen Energy. 2011;36:10141-8.
[15] Fernández-Sousa R, Betegón C, Martínez-Pañeda E. Analysis of the influence of microstructural traps on hydrogen assisted fatigue. Acta Materialia. 2020;199:253-63.
[16] Laureys A, Claeys L, De Seranno T, Depover T, Van den Eeckhout E, Petrov R, et al. The role of titanium and vanadium based precipitates on hydrogen induced degradation of ferritic materials. Materials Characterization. 2018;144:22-34.
[17] Zhang S, Zhao Q, Liu J, Huang F, Huang Y, Li X. Understanding the effect of niobium on hydrogen-induced blistering in pipeline steel: A combined experimental and theoretical study. Corrosion Science. 2019;159.
[18] Kawakami K, Matsumiya T. Numerical analysis of hydrogen trap state by TiC and V_4C_3 in bcc-iron. ISIJ International. 2012;52:1693-7.
[19] Krause AM, Olsson PAT, Music D, Bjerkén C. Interstitial diffusion of hydrogen in M_7C_3 (M=Cr,Mn,Fe). Computational Materials Science. 2023;218:111940.
[20] Kawakami K, Matsumiya T. Ab-initio Investigation of Hydrogen Trap State by Cementite in bcc-Fe. ISIJ International. 2013;53:709-13.
[21] Hickel T, Nazarov R, McEniry EJ, Leyson G, Grabowski B, Neugebauer J. Ab Initio Based Understanding of the Segregation and Diffusion Mechanisms of Hydrogen in Steels. JOM. 2014;66:1399-405.
[22] Ma Y, Shi Y, Wang H, Mi Z, Liu Z, Gao L, et al. A first-principles study on the hydrogen trap characteristics of coherent nano-precipitates in α-Fe. International Journal of Hydrogen Energy. 2020;45:27941-9.
[23] Li Y, Zhang X, Wu T, Tang J, Deng L, Li W, et al. First-principles study on the dissolution and diffusion behavior of hydrogen in carbide precipitates. International Journal of Hydrogen Energy. 2021;46:22030-9.
[24] Hammer P, Romaner L, Razumovskiy V. Hydrogen trapping in mixed carbonitrides. Acta Materialia. 2024; in press: 119754.
[25] Di Stefano D, Nazarov R, Hickel T, Neugebauer J, Mrovec M, Elsässer C. First-principles investigation of hydrogen interaction with TiC precipitates in α-Fe. Physical Review B. 2016;93:184108.
[26] Wei FG, Tsuzaki K. Quantitative analysis on hydrogen trapping of TiC particles in steel. Metallurgical and Materials Transactions A. 2006;37:331-53.
[27] Pérez Escobar D, Wallaert E, Duprez L, Atrens A, Verbeken K. Thermal desorption spectroscopy study of the interaction of hydrogen with TiC precipitates. Metals and Materials International. 2013;19:741-8.
[28] Ohnuma M, Suzuki J-i, Wei F-G, Tsuzaki K. Direct observation of hydrogen trapped by NbC in steel using small-angle neutron scattering. Scripta Materialia. 2008;58:142-5.
[29] Malard B, Remy B, Scott C, Deschamps A, Chêne J, Dieudonné T, et al. Hydrogen trapping by VC precipitates and structural defects in a high strength Fe–Mn–C steel studied by small-angle neutron scattering. Materials Science and Engineering: A. 2012;536:110-6.
[30] Chen Y-S, Haley D, Gerstl SSA, London AJ, Sweeney F, Wepf RA, et al. Direct observation of individual hydrogen atoms at trapping sites in a ferritic steel. Science. 2017;355:1196-9.
[31] Chen Y-S, Niu R, Liu P-Y, Burr P, Cairney J. Direct Observation of Hydrogen Distribution in Pearlite. Microscopy and Microanalysis. 2022;28:1618-20.
[32] Samanta S, Gangavarapu S, Jayabalan B, Makineni SK, Dutta M, Singh SB. Atomic-scale investigation of H-trapping by fine NbC precipitates in a low C ferritic steel. Scripta Materialia. 2023;234:115537.

[33] Boot T, Kumar AS, Eswara S, Kömmelt P, Böttger A, Popovich V. Hydrogen trapping and embrittlement of titanium and vanadium carbide containing steels after high temperature hydrogen charging. 2023;submitted.
[34] Sagar S, Sluiter MHF, Dey P. First - Principles study of hydrogen - Carbide interaction in bcc Fe. International Journal of Hydrogen Energy. 2023.
[35] Ding H, Fan X, Li C, Liu X, Jiang D, Wang C. First-principles study of hydrogen storage in non-stoichiometric TiC_x. Journal of Alloys and Compounds. 2013;551:67-71.
[36] Salehin R, Thompson GB, Weinberger CR. Hydrogen trapping and storage in the group IVB-VIB transition metal carbides. Materials & Design. 2022;214:110399.
[37] Huang S, Tian J, Liu Y. Atomic study of hydrogen behavior in different vanadium carbides. Journal of Nuclear Materials. 2021;554:153096.
[38] Zhang B, Su J, Wang M, Liu Z, Yang Z, Militzer M, et al. Atomistic insight into hydrogen trapping at MC/BCC-Fe phase boundaries: The role of local atomic environment. Acta Materialia. 2021;208:116744.
[39] Echeverri Restrepo S, Di Stefano D, Mrovec M, Paxton AT. Density functional theory calculations of iron - vanadium carbide interfaces and the effect of hydrogen. International Journal of Hydrogen Energy. 2020;45:2382-9.
[40] Wei FG, Hara T, Tsuzaki K. Precise determination of the activation energy for desorption of hydrogen in two Ti-added steels by a single thermal-desorption spectrum. Metallurgical and Materials Transactions B. 2004;35:587-97.
[41] Drexler A, Depover T, Verbeken K, Ecker W. Model-based interpretation of thermal desorption spectra of Fe-C-Ti alloys. Journal of Alloys and Compounds. 2019;789:647-57.
[42] Takahashi J, Kawakami K, Kobayashi Y, Tarui T. The first direct observation of hydrogen trapping sites in TiC precipitation-hardening steel through atom probe tomography. Scripta Materialia. 2010;63:261-4.
[43] Wei FG, Tsuzaki K. Hydrogen absorption of incoherent TiC particles in Iron from Environment at High Temperatures. Metallurgical and Materials Transactions A. 2004;35:3155-63.
[44] Vandewalle L, Depover T, Verbeken K. Hydrogen trapping of carbides during high temperature gaseous hydrogenation. International Journal of Hydrogen Energy. 2023.
[45] Zhang B, Zhu Q, Xu C, Li C, Ma Y, Ma Z, et al. Atomic-scale insights on hydrogen trapping and exclusion at incoherent interfaces of nanoprecipitates in martensitic steels. Nature Communications. 2022;13:3858.
[46] Lin Y-C, McCarroll IE, Lin Y-T, Chung W-C, Cairney JM, Yen H-W. Hydrogen trapping and desorption of dual precipitates in tempered low-carbon martensitic steel. Acta Materialia. 2020;196:516-27.
[47] Jin X, Xu L, Yu W, Yao K, Shi J, Wang M. The effect of undissolved and temper-induced (Ti,Mo)C precipitates on hydrogen embrittlement of quenched and tempered Cr-Mo steel. Corrosion Science. 2020;166:108421.
[48] Hammer P, Scheiber D, Ecker W, Romaner L, Moitzi F, Galler M, et al. Atomistic Modelling of Hydrogen Trapping on Coherent and Semi-coherent Ti-based Carbonitrides and Mixed-Metal Carbides in bcc Fe. In: Meseure K, editor. 4th International Conference on Metals Hydrogen. Ghent: Duprez, Lode;; 2022. p. L03.
[49] Wei FG, Hara T, Tsuzaki K. Nano-precipitates design with hydrogen trapping character in high strength steels. In: Somerday BP, Sofronis P, Jones RH, editors. International Hydrogen Conference: Effects of Hydrogen on Materials. Wyoming, USA: ASM International; 2008. p. 448-55.
[50] Wei FG, Tsuzaki K. Hydrogen trapping character of nano-sized NbC precipitates in tempered martensite. In: Somerday BP, Sofronis P, Jones RH, editors. International Hydrogen Conference: Effects of hydrogen on materials. Wyoming, USA: ASM International; 2008. p. 456-63.
[51] Wallaert E, Depover T, Arafin M, Verbeken K. Thermal Desorption Spectroscopy Evaluation of the Hydrogen-Trapping Capacity of NbC and NbN Precipitates. Metallurgical and Materials Transactions A. 2014;45:2412-20.

[52] Shi R, Ma Y, Wang Z, Gao L, Yang X-S, Qiao L, et al. Atomic-scale investigation of deep hydrogen trapping in NbC/α-Fe semi-coherent interfaces. Acta Materialia. 2020;200:686-98.
[53] Chen Y-S, Lu H, Liang J, Rosenthal A, Liu H, Sneddon G, et al. Observation of hydrogen trapping at dislocations, grain boundaries, and precipitates. Science. 2020;367:171-5.
[54] Drexler A, Depover T, Leitner S, Verbeken K, Ecker W. Microstructural based hydrogen diffusion and trapping models applied to Fe–C X alloys. Journal of Alloys and Compounds. 2020;826:154057.
[55] Drexler A, Vandewalle L, Depover T, Verbeken K, Domitner J. Critical verification of the Kissinger theory to evaluate thermal desorption spectra. International Journal of Hydrogen Energy. 2021;46:39590-606.
[56] Turk A, San Martín D, Rivera-Díaz-del-Castillo PEJ, Galindo-Nava EI. Correlation between vanadium carbide size and hydrogen trapping in ferritic steel. Scripta Materialia. 2018;152:112-6.
[57] Takahashi J, Kawakami K, Kobayashi Y. Origin of hydrogen trapping site in vanadium carbide precipitation strengthening steel. Acta Materialia. 2018;153:193-204.
[58] Takahashi J, Kawakami K, Tarui T. Direct observation of hydrogen-trapping sites in vanadium carbide precipitation steel by atom probe tomography. Scripta Materialia. 2012;67:213-6.
[59] Vandewalle L, Depover T, Verbeken K. Study of hydrogen trapping at carbides after gaseous charging at elevated temperatures. International Conference of Structural Integrity. Funchal, Portugal: Procedia Structural Integrity; 2023.